Cooperative Robotic Structure Mapping Using Wireless Measurements – A Comparison of Random and Coordinated Sampling Patterns

Alejandro Gonzalez-Ruiz and Yasamin Mostofi
Department of Electrical and Computer Engineering
University of California Santa Barbara, Santa Barbara, California 93106, USA
Email: {agon,ymostofi}@ece.ucsb.edu

Abstract – In this paper, we consider a mobile robotic network that is tasked with building a map of the objects/obstacles in an environment. We are interested in the see-through mapping of the obstacles, i.e., a mapping approach that can build the spatial variations of the occluded structures. We consider two cooperative mapping approaches based on making a small number of *random* or *coordinated* wireless channel measurements between pairs of robots. Our preliminary past work suggested that the coordinated approach may perform better than the random case. In this paper, it is our goal to 1) better understand if and to what extend this is correct and 2) validate our findings with a robotic experiment. More specifically, we show that the right approach for comparing the coordinated and random sampling patterns is to look at this problem from the perspective of optimizing the number/choice of the angular motion directions. In particular, random sampling can be considered as an asymptotic case where the total number of given wireless measurements are randomly distributed over an infinite number of angles. We then establish that the total number of available channel measurements should be distributed over a small number of angles, that is bigger than or equal to the number of jump angles of the structure, with a preference given to the angles of jumps. Finally and most importantly, we validate our findings by mapping occluded structures on our campus, based on only wireless channel measurements and by using our experimental robotic setup.

I. Introduction

Over the past few years, considerable progress has been made in the area of mobile sensor networks [2]–[14]. Such networks can play a key role in areas such as emergency response, surveillance and security, and battlefield operations. Accurate mapping of the obstacles/objects is key to the robust operation of unmanned autonomous networks. The obstacle/object map can be a 2D (or 3D) map of the environment, where we have zeros at locations where there is no obstacle and non-zero values at obstacle locations. In several scenarios, it also becomes important to have "see-through capabilities" and map the objects without direct sensing. For instance, the robotic vehicles may need to build an understanding of the objects inside a room, before entering it. Having see-through capabilities saves the overall obstacle mapping time and energy, by eliminating the need to sense all the objects directly.

In general, devising see-through mapping strategies, i.e. mapping without direct sensing, can be considerably challenging. In most related mapping work, such as Simultaneous Localization and Mapping (SLAM), only areas that are directly sensed are mapped [15]–[19]. Similarly, approaches based on generating an occupancy map also address reducing the uncertainty of direct sensing [20], [21]. However, areas that are not sensed directly are not mapped. In the wireless communication literature, it is well-established that the shadowing component of a wireless transmission contains implicit information on the objects located on the path between the transmitter and receiver [22]. Thus, wireless measurements, between pairs of robots, can possibly be utilized for non-invasive obstacle mapping. Along this line, in [23]–[25], we proposed a framework for compressive obstacle/object mapping in robotic networks, with see-through capabilities, based on making a few wireless channel measurements. Wireless-based detection has also been explored. For instance, in [26], authors use a transmitter that is buried underground and several fixed receivers on the surface to detect underground tunnels/facilities using radar. Similarly, in [27], [28], the authors build a network of several dozen fixed sensors in order to track a person, based on making several measurements between pairs of sensors.

Our past work on wireless-based obstacle mapping was mainly based on making coordinated wireless measurements. In a coordinated approach, the transmitting (TX) and receiving (RX) robots make wireless measurements while following a coordinated motion pattern over a number of angles. This, however, may not be feasible due to environmental constraints. In a random-sampling approach, on the other hand, the TX/RX robots can take any arbitrary position and do not have to follow any specific motion pattern, as we defined in [1]. Our preliminary simulation results of [24] suggested that the coordinated sampling case may perform better than the random one. In this paper, we are motivated by our past work and want to thoroughly understand and compare the performance of the *coordinated* and *random* sampling approaches. We show that the right approach for comparing the performance of these two motion-sampling patterns is to consider the relationship

This work is supported by NSF CAREER award # 0846483. A very small part of this work appeared in the IEEE conference Milcom 2010 [1].

between the reconstruction quality and the angular directions where the map is sampled. More specifically, we show that the total number of available channel measurements should be distributed over a small number of angles (bigger than or equal to the number of jump angles of the structure), with a preference given to the angles of jumps. This suggests that the coordinated approach does not necessarily have a better performance than the random case unless the jump angles are chosen. We also validate our findings in an experimental setup that can involve environmental constraints.

In general, extracting the obstacle information without making a prohibitive number of wireless transmissions, is considerably challenging. In order to address this and enable the mapping, based on a small number of wireless transmissions, we utilize the new theories of compressive sensing [29], [30]. The impact of multipath fading further makes our wireless-based mapping considerably challenging. Following the same approach of [24], we use adaptive narrow beamwidth antennas to limit the impact of multipath fading. Using our experimental robotic platform, we then show the performance of both approaches in mapping real structures on our campus and having see-through capabilities, based on only making a few wireless measurements.[1]

The rest of the paper is organized as follows. In Section II, we provide a brief overview of the area of compressive sampling, as relevant to this paper. In Section III, we explain the foundation of our wireless-based mapping and introduce the random and coordinated approaches. In Section IV, we show the performance and the underling tradeoffs of the two approaches, using both simulation and experimental results. We conclude in Section V.

II. A Brief Overview of Compressive sampling theory [29]–[31]

Consider a scenario where we are interested in recovering a vector $x \in \mathbb{R}^N$. For 2D signals, vector x can represent the columns of the matrix of interest stacked up to form a vector. Let $y \in \mathbb{R}^K$ represent the incomplete linear measurements of vector x, where $K \ll N$. We have

$$y = \Phi x, \tag{1}$$

where Φ is the observation matrix. Since $K \ll N$, the system is severely under-determined and we can not uniquely solve for x based on the observation set y. However, suppose that x has a sparse representation in another domain: $x = \Gamma X$, where Γ is an invertible matrix and X is S-sparse, i.e. $|\text{supp}(X)| = S \ll N$. This implies that the number of non-zero elements in X is considerably smaller than N. Then we will have

$$y = \Psi X, \tag{2}$$

where $\Psi = \Phi \times \Gamma$. In general, solving for vector X requires solving the following non-convex combinatorial problem:

$$\min ||X||_0, \text{ subject to } y = \Psi X, \tag{3}$$

where $||X||_0$ denotes the zero norm of vector X. The computational complexity of solving this problem, however, can be very high. Recently, there have been several breakthroughs in solving this problem with a considerably lower computation. Specifically, consider the following relaxation of the aforementioned ℓ_0 optimization problem:

$$\min||X||_1, \text{ subject to } y = \Psi X. \tag{4}$$

This ℓ_1 relaxation, under certain conditions, can exactly recover X from the measurement vector y [29]. In our case, we are interested in reconstructing an obstacle map. Thus, the spatial variations of the map (gradient) are also considerably sparse. In such cases, another related sparsity-based reconstruction approach is to use the sparsity in the gradient [29], [32], [33]. Let $f = [f_{i,j}]$ denote an $m \times m$ matrix that represents the spatial function of interest. Define the following operators: $D_{h,i,j}(f) = \begin{cases} f_{i+1,j} - f_{i,j} & i < m \\ f_{i,j} - f_{1,j} & i = m \end{cases}$ and $D_{v,i,j}(f) = \begin{cases} f_{i,j+1} - f_{i,j} & j < m \\ f_{i,j} - f_{i,1} & j = m \end{cases}$. Then, the Total Variation (TV) function is defined as follows:

$$\text{TV}(f) = \sum_{ij} \|D_{i,j}(f)\|, \tag{5}$$

where $D_{i,j}(f) = [D_{h,i,j}(f) \quad D_{v,i,j}(f)]$, and the $\|.\|$ operator can either represent the ℓ_1 norm, corresponding to the anisotropic discretization of TV, or the ℓ_2 norm, corresponding to the isotropic discretization of TV. TV minimization approaches then solve the following problem or a variation of it:

$$\min \text{TV}(f), \text{ subject to } y = \Psi_f \times X, \tag{6}$$

where X is a column vector that results from stacking up the columns of matrix f, and y is the observation vector, which is linearly related to X through matrix Ψ_f. In [34], the authors show that solving Eq. 6, based on both isotropic and anisotropic TV, results in a similar reconstruction. We have also observed that at the low sampling rates used in this paper, anisotropic and isotropic TV yield very similar results, in terms of speed of convergence and reconstruction quality. Consequently, unless we specifically indicate otherwise, the results of this paper are based on using anisotropic TV.

The concept of Total Variation was first introduced in [35] for image denoising. TV minimization is a variant of ℓ_1 relaxation that tends to give sharper results on certain types of signals [36], and is effective in restoring signals that have staircase characteristics [37]. Thus, it is especially appropriate for the recovery of obstacle maps since the borders, separating different objects, result in sharp discontinuities. Recently, TVAL3 (TV Minimization by Augmented Lagrangian and Alternating Direction Algorithms) is proposed for solving the TV minimization problem efficiently and robustly, which we will use extensively in this paper [33].

III. Compressive Cooperative Mapping of Obstacles

In this section we show how a group of mobile nodes can build a map of obstacles, including occluded ones, by using only wireless measurements. We start by summarizing the work of Mostofi et al. for obstacle mapping based on wireless

[1]It should be noted that wireless-based mapping is not a replacement for the current obstacle mapping techniques but rather a complement, by providing the additional see-through capability.

measurements [1], [23], [24]. We then discuss and compare the two approaches of random and coordinated mapping, address the optimum number and choice of the measurement angles, and most importantly show the performance with an experimental setup. We consider building a 2D map of the obstacles in this paper. This means that for real 3D structures, we reconstruct a horizontal cut of them. However, our proposed approach can be easily extended to 3D maps.

Figure 1 shows a sample 2D obstacle map where a number of vehicles want to map the space before entering it. Let $g_n(u,v)$ represent the binary map of the obstacles at position (u,v) for $u,v \in \mathbb{R}$. We have

$$g_n(u,v) = \begin{cases} 1 & \text{if } (u,v) \text{ is an obstacle} \\ 0 & \text{else} \end{cases} \quad (7)$$

Consider the received signal strength in communication from Transmitter1 to Receiver1 in Fig. 1. As it is well established, there are three dynamics associated with the spatial variations of the channel quality and therefore the received signal strength [22], [38], as indicated in Fig. 2. The slowest dynamic is associated with the signal attenuation due to the distance-dependent power fall-off (path loss). Then there is a faster variation referred to as shadow fading (shadowing), which is due to the impact of the blocking objects. This means that each obstacle along the transmission path leaves its mark on the received signal by attenuating it to a certain degree, characterized by its properties. Finally, depending on the receiver antenna angle, multiple replicas of the transmitted signal can arrive at the receiver, due to the reflection from the surrounding objects, resulting in multipath fading, a faster variation in the received signal power [39], [40]. The shadowing component of the communication from Transmitter1 to Receiver1, therefore, contains implicit information of the obstacles along the communication path.

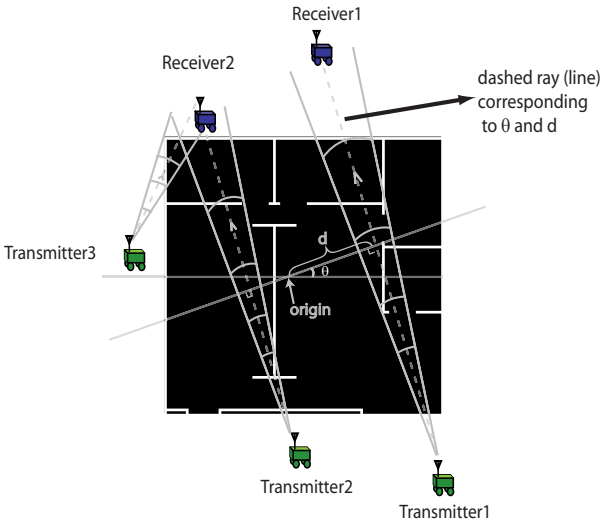

Fig. 1. An indoor obstacle map with the obstacles marked in white and the illustration of compressive cooperative mapping, using coordinated wireless measurements (case of Transmitter1/Receiver1 and Transmitter2/Receiver2) and random wireless measurements (case of Transmitter1/ Receiver1 and Transmitter3/Receiver2).

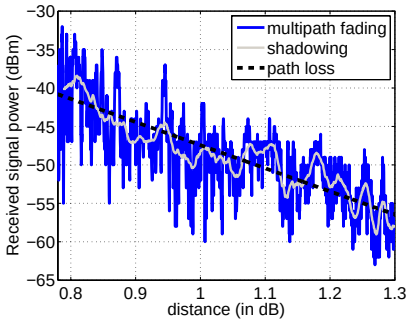

Fig. 2. A real channel measurement and the corresponding three underlying dynamics.

Consider the dashed ray (line) that corresponds to distance d and angle θ in Fig. 1. This line is at distance d from the origin and is perpendicular to the line that is at angle θ with the x-axis. Let $P(\theta,d)$ represent the received signal power in the transmission along this ray.[2] We can model $\ln P(\theta,d)$ as follows

$$\ln P(\theta,d) = \underbrace{\ln P_T}_{\substack{\text{transmitted} \\ \text{power in dB}}} + \underbrace{\beta_{\text{dB}} - \alpha \ln l(\theta,d)}_{\text{path loss } (\leq 0)} + \underbrace{\sum_i r_i(\theta,d) n_i(\theta,d)}_{\substack{\text{shadowing effect due to} \\ \text{blocking objects}(\leq 0)}} + \underbrace{w_{\text{dB}}(\theta,d)}_{\text{multipath fading}}, \quad (8)$$

where P_T represents the transmitted power, β_{dB} is a constant that is a function of system parameters, α is the degradation exponent of the wireless signal and $l(\theta,d)$ is the distance between the transmitter and receiver across that ray. For the shadowing term, r_i is the distance travelled across the i^{th} object along the (θ,d) ray, $n_i < 0$ is the decay rate of the wireless signal within the i^{th} object, and the summation is over the objects across that line. As can be seen, shadowing characterizes wireless signal attenuation as it goes through the obstacles along the transmission path and therefore contains information about the objects along that line. The impact of multipath fading is modeled by $w_{\text{dB}}(\theta,d) = \ln w(\theta,d)$ where $w(\theta,d)$ is a positive random variable with unit average. Then we have

$$\begin{aligned} h(\theta,d) &\triangleq \ln P(\theta,d) - \ln P_T - \left(\beta_{\text{dB}} - \alpha \ln l(\theta,d)\right) \\ &= \underbrace{\sum_i r_i(\theta,d) n_i(\theta,d)}_{\text{shadow fading effect}} + \underbrace{w_{\text{dB}}(\theta,d).}_{\text{multipath fading}} \end{aligned} \quad (9)$$

By using an integration over the line that corresponds to θ and d, we then have:

$$h(\theta,d) = \int\int_{\text{line } (\theta,d)} g(u,v) du dv + w_{\text{dB}}(\theta,d), \quad (10)$$

where

$$g(u,v) = \begin{cases} n(u,v) & \text{if } g_n(u,v) = 1 \\ 0 & \text{else} \end{cases} \quad (11)$$

[2]We assume negligible receiver thermal noise in our formulation. However, our experimental results naturally experience receiver thermal noise as well as other noise sources.

with $g_n(u,v)$ representing the binary map of the obstacles, as indicated by Eq. 7, and $n(u,v)$ denoting the decay rate of the signal inside the object at position (u,v) (see $n_i(\theta,d)$ in Eq. 8). $g(u,v)$ then denotes the true map of the obstacles including wireless decay rate information. This is what the cooperative mobile nodes need to reconstruct based on pair-wise wireless measurements.[3]

Our compressive cooperative obstacle mapping framework uses the fact that $h(\theta,d)$ contains implicit information on the traversed obstacles. However, it is challenging to obtain g from a very few wireless measurements. In order to make this possible, we use the aforementioned theories of compressive sensing, which allow us to extract this information based on sparse wireless measurements. The impact of multipath fading further makes the reconstruction considerably challenging. In order to address this and limit the impact of multipath fading, we use adaptive directional antennas, with a small beamwidth (angle), for both the transmitting and receiving robots [24]. Here is a summary of our experimental setup.

A. A Summary of the Experimental Robotic Platform and the Impact of Multipath Fading

In our experimental setup, we use a number of Pioneer P3-AT mobile robots [41]. We have equipped each robot with a directional narrow-beam antenna, from Laird [42], which is crucial in limiting the impact of multipath fading. Each antenna has a 21° horizontal and a 17° vertical beamwidth, a 15 dBi gain and is suitable for IEEE 802.11b/g applications. We have further developed the needed servo control hardware and software for automated antenna rotation, angle control and alignment so the TX and RX robots can stay aligned during the mapping operation. Each robot is equipped with an IEEE 802.11g wireless card and can record the received signal strength as it moves. Fig. 3 (left) shows the resulting platform with the directional antenna mounted, while the right figure shows two of our robots making wireless measurements in order to see through the walls and reconstruct the obstacle.

Fig. 3. (left) A pioneer 3-AT robot equipped with our servo control mechanism/fixture and an adaptive narrow-beam directional antenna and (right) two robots in action on our campus, making wireless measurements in order to map the obstacle.

Since our mathematical modeling of a wireless transmission can not embrace all the propagation phenomena, we do not expect a perfect recovery with a very small number of wireless measurements in a real environment. However, as long as the reconstruction is informative, for the cooperative operation of the robots, it could be considerably valuable. Next, we develop the details of obstacle mapping based on both coordinated and random wireless measurements.

B. Coordinated Wireless Measurements

Consider the line (ray) that passes through Transmitter1/Receiver1 in Fig. 1. In the coordinated case, two vehicles move outside of the structure, in a coordinated fashion, such that the angle of their corresponding ray stays perpendicular to the line that passes through the origin at angle θ. A number of wireless channel measurements are then made at different ds (both positive and negative). We say that the robots are making measurements at angle θ in this case. The positions indicated by Transmitter1/Receiver1 and Transmitter2/Receiver2, for instance, are two examples of coordinated measurements at angle θ. The robots then repeat the process for other θs. For a given angle θ_i, we define a set of ordered ds where measurements are taken, as follows: $D_i = \{d_1(\theta_i), d_2(\theta_i), \ldots, d_{N_i}(\theta_i)\}$, where N_i denotes the total number of gathered measurements at angle θ_i. In this paper, we only consider periodic coordinated measurements with respect to d, due to space limitations.[4] In other words, we consider the case where the measurements are such that for all i, the distance $\Delta d_j(\theta_i) = d_{j+1}(\theta_i) - d_j(\theta_i)$, for $1 \leq j \leq N_i - 1$, is a constant denoted by Δd. Without loss of generality, we assume that $d_{j+1}(\theta_i) > d_j(\theta_i)$.

In practice, the parameters of the path loss component of the received signal in Eq. 8 can be estimated by using a few Line Of Sight (LOS) transmissions in the same environment, as we have shown in [39], [40]. Therefore, the impact of path loss can be removed and the receiving robot can calculate $h(\theta,d)$. Thus, for each θ and d pair, a wireless transmission and reception is made, which results in measuring a line integral of Eq. 9. Then f of Eq. 6 is the spatially-discretized version of g of Eq. 11. Let X of Eq. 2 be the vector representation of f, where the columns are stacked up to form a vector. Let vector y_c denote the vector of the gathered samples of $h(\theta,d)$ of Eq. 9, using coordinated measurements. We have $y_c = \Psi_c X + e$, where e models the impact of multipath fading and measurement noise. In each row of Ψ_c, the non-zero elements correspond to the obstacle map pixels that the corresponding ray visited, with each non-zero value indicating the distance travelled in the corresponding pixel.[5] We then use the sparsity in the spatial variations (TV) in order to reconstruct the obstacle map, as discussed in Section II.[6]

[3]Note that we do not assume any knowledge on n in our reconstructions. In other words, our approach needs to solve for n. Furthermore, we do not assume any a priori knowledge on the heterogeneity or homogeneity of the structure.

[4]The observations of this paper are also equally applicable to the case of non-periodic coordinated sampling.

[5]We can also approximate the distance travelled in each pixel by the size of a side of a pixel as long as the designated resolution of the map is not too low. This can simplify our modeling and reconstruction, which is what we do in the next section.

[6]It should be noted that there are other compressive sensing approaches for reconstructing the obstacle map, based on coordinated measurements. For instance, sampling in the frequency domain and sparsity in the wavelet can also be utilized (for the same measurement vector), as we proposed in [24]. In [24], we showed that the approach described in this section, i.e. space sampling and TV sparsity, provides a performance better than or comparable to other approaches, but with the lowest computational complexity. Thus, we use this approach in this paper.

We know from the compressive sampling literature, especially in the context of ℓ_0 and ℓ_1 optimization problems, that a minimum number of measurements is needed to find the correct solution. For our TV-based coordinated obstacle mapping approach, we can easily see this with a counter example.

Definition 1 - Horizontal Wall Map: We define a *Horizontal Wall Map* as a discretized obstacle map f of size $m \times m$ pixels where a homogeneous horizontal wall of length p pixels, for $2 \leq p < m$, is placed along the kth row of f, with no obstacles anywhere else.

Lemma 1: Consider the case where $e = 0$. The TV minimization of the spatial variations of the obstacle map based on the coordinated wireless measurements $y_c = \Psi_c \times X + e$, may not result in the correct solution if the number of gathered measurements is too low or the sampling motion angles are not chosen properly.

Proof: Consider the scenario where the Horizontal Wall Map is sampled with coordinated wireless channel measurements along $\theta = 90°$, such that one measurement is taken along each of the m rows of f. Without loss of generality, we assume that the decay rate of the wireless signal inside the obstacle structure is equal to 1, i.e. $n = -1$ in Eq. 11 and $f_{i,j} \in \{0, 1\}\ \forall i, j \in \mathbb{Z},\ 1 \leq i, j \leq m$. Let X be the vector representation of the discrete obstacle map f. Also let Ψ_{90} denote the corresponding measurement matrix and y_{90} represent the resulting measurement vector. We have the following minimization problem:

$$\min \text{TV}(f),\ \text{subject to } y_{90} = \Psi_{90} \times X. \tag{12}$$

Let $[y_{90}]_i$ be the ith component of y_{90}. Note that $[y_{90}]_i = 0\ \forall i \neq k$, and $[y_{90}]_k = p$. Thus, the feasible solutions are such that $f_{i,j} = 0\ \forall (i, j), i \neq k$. The TV of the recovered map can then be characterized as follows where $f_{i,j}$ is the value of the pixel at the i^{th} row and j^{th} column of f:

$$\begin{aligned} &TV(f) \\ &= 2(f_{k,1} + f_{k,2} + \ldots + f_{k,m}) \\ &\quad + |f_{k,1} - f_{k,2}| + |f_{k,2} - f_{k,3}| + \ldots + |f_{k,m} - f_{k,1}| \\ &= 2p + |f_{k,1} - f_{k,2}| + |f_{k,2} - f_{k,3}| + \ldots + |f_{k,m} - f_{k,1}|. \end{aligned} \tag{13}$$

It can be seen that for this case, $TV(f)$ is minimized if and only if $f_{k,1} = f_{k,2} = \ldots = f_{k,m} = \frac{p}{m}$. However, it does not correspond to the original map f where the kth row has $p < m$ pixels equal to 1 and $m - p$ pixels equal to 0. ■

C. Random Wireless Measurements

Due to the environmental constraints, it may not always be possible to make coordinated measurements. For instance, the path where the robots need to move for making coordinated measurements may be partially blocked. In such cases, the robots can make measurements at different θ and d pairs that are chosen randomly, without trying to maintain a specific pattern. In Fig. 1, the positions indicated by Transmitter1/Receiver1 and Transmitter3/Receiver2, for instance, indicate an example of such a case. Similar to the coordinated case, we have $y_r = \Psi_r X + e$, where vector y_r denotes the gathered samples of $h(\theta, d)$ of Eq. 9, using random measurements and Ψ_r is similar to Ψ_c, except that in this case it does not have the coordinated structure. Similar to the previous case, we use the sparsity in the spatial variations (TV) for map reconstruction. While the performance of the coordinated approach in mapping real occluded structures was shown in [24], the performance based on random wireless measurements has not been shown before, which is one of the goals of this paper.

IV. Coordinated or Random Wireless Measurements?

So far we have discussed two approaches for obstacle mapping, using random and coordinated sparse wireless measurements. By incorporating a random offset in the range $[0, \Delta d)$ to the start position of the first coordinated measurement sample along each angle, the case of random sampling can indeed be considered as a special case of coordinated, when the total number of available measurements are randomly distributed among an infinite number of angles. Based on this approach, in this section we compare the performance of the two approaches and show the underlying tradeoffs, using both simulation and experimental results. More specifically, we discuss the optimum number of measurement angles, as well as the choice of angles, to distribute a given number of measurements. We furthermore show the performance of both approaches, in an experimental setup that involves environmental constraints.

In order to motivate our discussion, we start by comparing the performance of the random and coordinated approaches, in a simulation environment, where we can directly simulate $h(\theta, d)$ of Eq. 9, without the impact of multipath fading. This is then followed by our experimental results. Consider the problem of reconstructing the T-shaped structure of Fig. 4 (right). Fig. 5 shows this reconstruction, in a simulation environment, where only 0.77% measurements are taken. This sampling rate denotes the total number of wireless transmissions divided by the size of the 2D map in pixels (in percentage) [23]. For the coordinated case of the left figure, all the measurements are made periodically along one angle ($\theta = 0°$ with the x-axis in this case) while the right figure corresponds to the case of random measurements, i.e. the measurements are randomly distributed over a very high number of angles.[7] It can be seen that the random case performs better than the coordinated one, in this case, since it measures the object from different angles. However, neither of these two cases provide a good enough reconstruction quality. Then, we have the following question: given a total number of possible pairwise wireless measurements, what is the optimum number of angles (optimum in terms of reconstruction quality) to distribute the measurements over? If the optimum number of angles becomes very large, then a more randomized strategy becomes appropriate. Before we can answer this question, however, we need to address the choice of optimum angles.

Consider a structure whose layout corresponds to Fig. 6 (left), which has walls laid out along seven different angles.

[7]Note that for the random case it is not necessary for each angle to have at least one measurement.

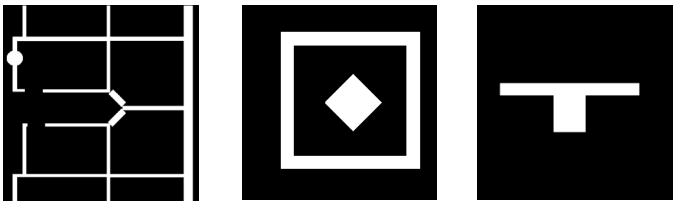

Fig. 4. Obstacle maps corresponding to (left) a section of the basement of our building, (center) a blocked diamond-shaped column and (right) a T-shaped column.

Fig. 5. Comparison of our mapping framework in the reconstruction of the T-shaped structure of Fig. 4, at 0.77% sampling rate, with (left) coordinated samples distributed over one angle and (right) random sampling.

Consider the case where two robots are making coordinated measurements, along a given number of angles in this environment. If the robots can freely choose the angles across which to make wireless measurements, then it is intuitive that the angles that correspond to the directions of the most changes (jumps) in h of Eq. 10 should be sampled first. Fig. 6, for instance, shows the case where the robots can make a given number of wireless measurements across a given number of angles. The figure shows the impact of choosing some (or all) of the measurement angles to be along the directions of jumps. It can be seen that as the robots make more coordinated measurements along the directions of jumps, the performance improves considerably. While proving this mathematically for a general map is beyond the scope of this paper, we provide a simple proof for the case of Horizontal Wall Map defined in section III-B.

Lemma 2: Consider the Horizontal Wall Map of Definition 1 and the case where $e = 0$. Then, sampling along the angle where the majority of the jumps occur ($\theta = 90^\circ$) provides a better reconstruction quality than sampling along $\theta = 0^\circ$. Furthermore, if a binary constraint is enforced in the reconstruction, the samples at $\theta = 90^\circ$ provide more information.

Proof: Similar to the proof of Lemma 1 and without loss of generality, we assume that the decay rate of the wireless signal inside the obstacle structure is equal to 1, i.e. $n = -1$ in Eq. 11. Consider the scenario of Lemma 1, where the Horizontal Wall Map is sampled with coordinated wireless channel measurements along $\theta = 90^\circ$, such that one measurement is taken along each of the m rows of f. Let Ψ_{90} and y_{90} be as defined in Lemma 1 for this case. By using the result of Lemma 1, we can calculate the reconstruction error variance when sampling along $\theta = 90^\circ$ as follows:

$$E_{90} \quad = \quad \left(\frac{p}{m} - 1\right)^2 p + \frac{p^2}{m^2}(m-p) = p - \frac{p^2}{m}. \quad (14)$$

Next, consider the case where coordinated wireless channel measurements are made along $\theta = 0^\circ$, such that one measurement is taken along each column of f. After a few lines of derivations, we can confirm that we have the following error variance for this case:

$$E_0 \quad = \quad \left(\frac{1}{m} - 1\right)^2 p + \frac{1}{m^2}(mp - p) = p - \frac{p}{m}. \quad (15)$$

Clearly, $E_{90} < E_0$.

If we further place a constraint on the TV minimization problem that forces the solution to be binary for each pixel (this would be the case if we knew n a priori), then the solution may not be unique for the aforementioned two cases. In this case, we can further analyze the amount of information that each of the sampling patterns provides as follows. Consider a binary map f^{bin} with 0.5 probability of having an obstacle at each of the 2^{m^2} pixels. Let $X_{f^{\text{bin}}}$ represent the random vector of the stacked columns of the map and also let $X_{f^{\text{bin}},\theta}$ represent the random vector of the map conditioned on the gathered wireless measurements along angle θ. We can easily confirm that,

$$\begin{aligned} &I(X_{f^{\text{bin}}}, X_{f^{\text{bin}},\theta=90^\circ}) \\ &= H(X_{f^{\text{bin}}}) - H(X_{f^{\text{bin}}}|X_{f^{\text{bin}},\theta=90^\circ}) \\ &= m^2 - \log_2 \binom{m}{p}, \end{aligned} \quad (16)$$

where I and H are the mutual information and the entropy respectively. On the other hand, if the samples are such that $\theta = 0^\circ$, then,

$$I(X_{f^{\text{bin}}}, X_{f^{\text{bin}},\theta=0^\circ}) = m^2 - p\log_2(m). \quad (17)$$

Since $\binom{m}{p} \leq \frac{m^p}{p!} \leq m^p$, we conclude that $I(X_{f^{\text{bin}}}, X_{f^{\text{bin}},\theta=90^\circ}) \geq I(X_{f^{\text{bin}}}, X_{f^{\text{bin}},\theta=0^\circ})$.

■

This observation is important, especially in mapping indoor environments, since there are typically a small number of jump angles (mainly perpendicular walls). Thus, if the environmental constraints allow it, then the directions with more jumps should be sampled first, for the case of coordinated mapping.

Consider the case where the robots can make a given number of coordinated wireless measurements. We next discuss the optimum number of angles, over which the given measurements should be distributed. In this way, we also compare the random and coordinated cases. In all these reconstructions, first the angles that correspond to the directions of jumps are chosen. The rest of the angles are then chosen so as to make the angle distribution as uniform as possible, while keeping the previously-chosen angles. For each angle, the measurements are distributed equally spaced with distance Δd. Furthermore, a random offset in the interval $[0, \Delta d)$ is used for the first measurement at each angle. Fig. 7 shows the mapping performance for the three structures of Fig. 4, where a total number of given measurements are distributed over a variable number of angles. As the number of angles increases, the randomness of mapping increases as well. As can be seen, for each structure, there is an optimum number of angles where the coordinated measurements should be distributed. For instance, for the middle and right structures

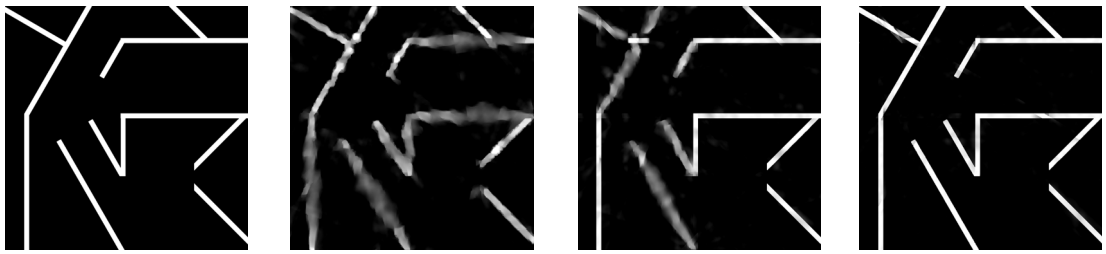

Fig. 6. (left) An obstacle map with discontinuities occurring at seven angles, (middle-left) reconstruction with no measurements along the jump angles, (middle-right) reconstruction with some measurements along the jump angles and (right) reconstruction with all the measurements along the jump angles.

of Fig. 4, the optimum number of angles is 4 whereas it is 10 for the left one.[8] The results suggest that the case of random measurements (equivalent to a very high number of angles) does not typically provide the best performance. Furthermore, the optimum number of angles is typically equal to or more than the number of jump angles of the structure. As the structure becomes more complicated (the left structure of Fig. 4), the given samples should be distributed over more angles. We have consistently observed these behaviors with other structures.

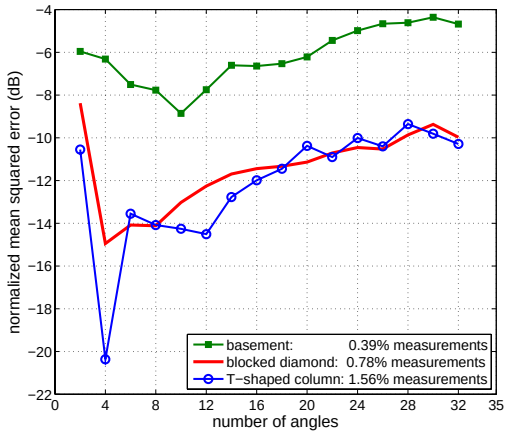

Fig. 7. Error curves for the reconstruction quality of the obstacle maps of Fig. 4, using our coordinated approach. As the number of angles increases, the randomness of mapping increases.

A. Comparison of the Mapping and See-Through Capabilities of the Coordinated and Random Cases – An Experimental Test

So far, we discussed the performance of the two approaches in a simulation environment, and also without considering environmental constraints. We next show the performance and see-through capabilities of the two approaches in mapping an obstacle structure (that includes an occluded part) on our campus. Figure 8 (left) shows a structure on our campus, with its horizontal cut shown in the center figure. For the coordinated case, two robots make coordinated movements and periodic measurements along lines with angles 0°, 90° (marked on the center figure), 45° and 135°. On the other hand, for the random case, the transmitting and receiving robots make wireless measurements at random positions along the dashed lines of Fig. 8 (right), while avoiding the cases where both the transmitting and receiving robots are on the same side of the structure. For the random case, we consider two scenarios of *unconstrained* and *constrained* mapping. In the former, the robots are free to position themselves anywhere outside of the structure and make measurements at any position along the dashed lines of Fig. 8 (right). In the latter, however, there are environmental constraints (marked in the right figure) that prevent the robots from moving along certain segments of the lines. In order to have a fair comparison, all the three approaches make the same number of wireless measurements.

Figure 9 shows the reconstruction performance for different sampling rates.[9] Each sampling rate denotes the total number of wireless transmissions divided by the size of the 2D map in pixels, as discussed before. The top and bottom rows show the performance for the two cases of 0.76% and 1.83% sampling rates respectively. The three columns show the mapping quality for the cases of coordinated, random unconstrained and random constrained measurements from left to right. As can be seen, the coordinated case, with measurements along four angles, performs considerably better than the random ones, as expected from the previous discussions of the paper. Even at a very low sampling rate of 0.76%, the occluded column can be clearly seen, in terms of its position and dimension. Furthermore, the random unconstrained case outperforms the constrained one, as expected. As the number of measurements increases, the reconstruction performance improves for all the cases. As mentioned earlier, we use anisotropic TV minimization approach and TVAL3 solver [33] for all these reconstructions. Fig. 10 compares the sampling rate needed in order for the random (unconstrained) approach to have a similar reconstruction quality (same MSE) to the coordinated one. As can be seen, a sampling rate of 6.98% (3.81 times more) is needed for the random case.

Fig. 11 then compares the performance of the coordinated and random approaches as a function of the sampling rate. The coordinated measurements are made along 0°, 90°, 45° and 135°, whereas the random cases make measurements at positions along the dashed lines of Fig. 8 (right), as explained before. As can be seen, the coordinated case outperforms the random ones.

[8]Note that this is independent of the existence of the column in the left figure, since its contribution to the overall structure is small.

[9]A threshold is applied to the reconstructed figures such that any value that is 10dB below the maximum is zeroed. This was done because we noticed that there could be scenarios where reconstructed pixels with very small values get magnified by some printers or monitors with certain gamma settings. A simple thresholding can avoid such cases.

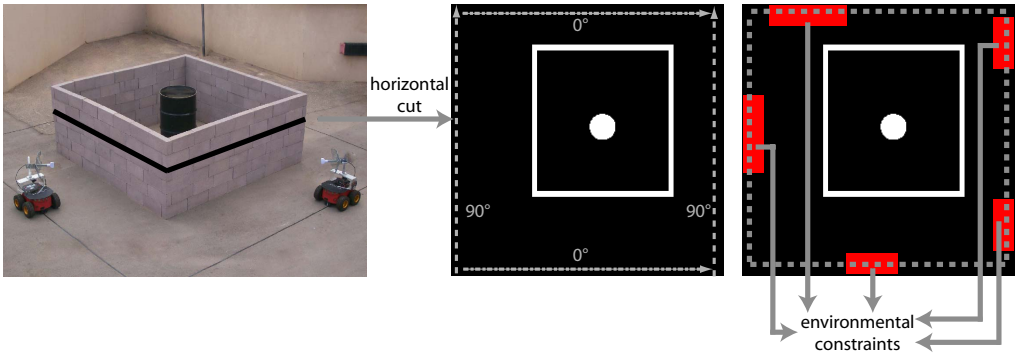

Fig. 8. (left) An obstacle structure on our campus, (center) its horizontal cut and (right) illustration of the physical constraints that limit the positioning of the robots for the constrained case. Our robots aim to reconstruct the structure, based on only making a few wireless transmissions from outside.

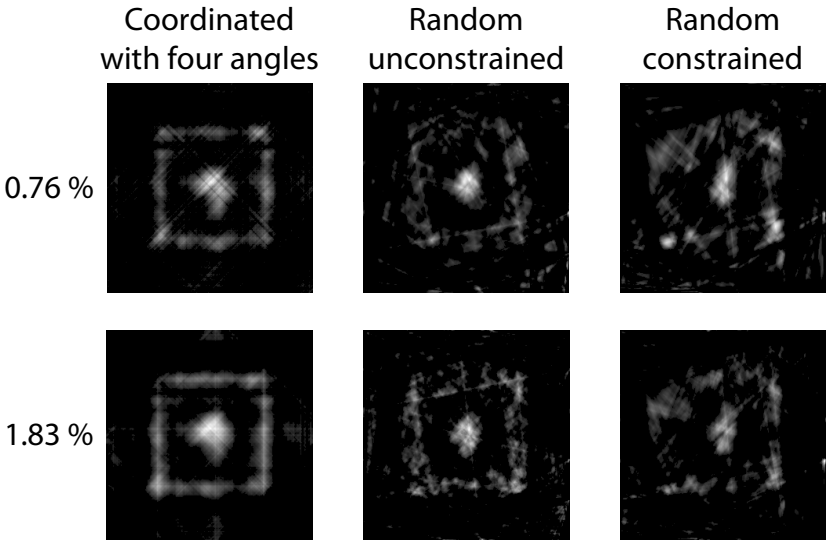

Fig. 9. Comparison of the mapping and see-through capabilities of the coordinated and random approaches in mapping the structure of Fig. 8, using our experimental robotic platform. The top and bottom rows show the performance for the two cases of 0.76% and 1.83% sampling rates respectively. The three columns show the mapping quality for the cases of coordinated (along four angles), random unconstrained and random constrained measurements from left to right. It can be seen that the mapping performance improves considerably from right to left.

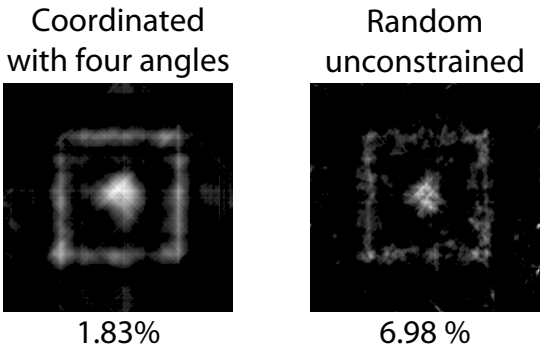

Fig. 10. Reconstruction of the structure of Fig. 8, with (left) coordinated sampling with 1.83% measurements along four angles and (right) random unconstrained sampling with 6.98% measurements. Both reconstructions result in the same Mean Squared Error (MSE).

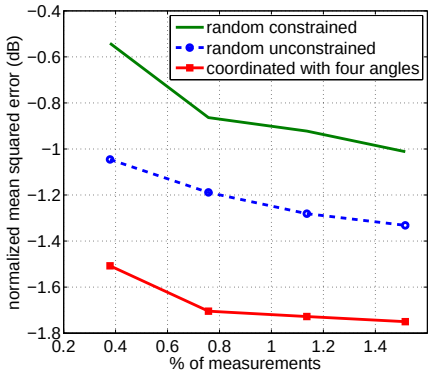

Fig. 11. Error curves for the reconstruction quality of the obstacle map of Fig. 8, using our coordinated approach along four angles and our random approaches. Even at very low sampling rates, the coordinated approach outperforms the random ones.

As we discussed earlier, the performance of the coordinated case depends heavily on the choice of the sampling angles. In Fig. 9, four angles including the jump ones were sampled, which resulted in the coordinated case performing better than the random one. However, the random case can perform better if the coordinated case is not sampled along the jump angles. The next experiment shows this in mapping the structure of Fig. 8. For the first set of measurements, the robots make measurements along the jump angles of the outer wall i.e. at 0° and 90°, while for the second set the measurements

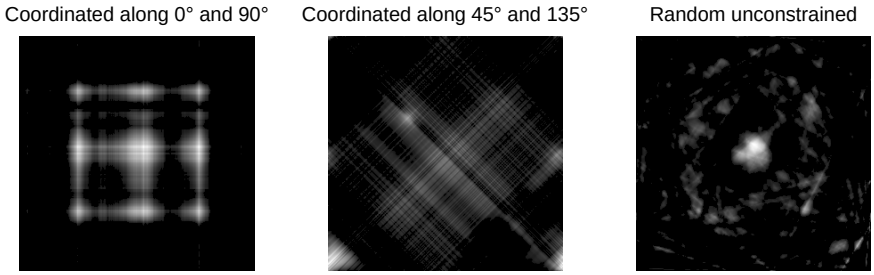

Fig. 12. Reconstruction of the structure of Fig. 8 with 0.76% measurements, with (left) coordinated sampling along the jump angles of the outer walls (0 and $90°$), (center) coordinated sampling along $45°$ and $135°$ and (right) random unconstrained sampling. It can be seen that random sampling can be more informative than coordinated if the structure is not sampled along the jump angles in the coordinated case.

are made along $45°$ and $135°$. As can be seen in Fig. 12 (center), making coordinated measurements along the angles that do not correspond to the jump angles does not result in a useful reconstruction as neither the outer walls nor the occluded obstacle can be correctly mapped. In contrast, if the jump angles are used, the location of the outer walls can be correctly detected, as seen in Fig. 12 (left). On the other hand, Fig. 12 (right) shows the reconstruction using unconstrained random wireless measurements at the same low sampling rate used for the coordinated cases (0.76%). As can be seen, the reconstruction is considerably better than the case of coordinated along $45°$ and $135°$ in Fig. 12 (center).

B. Practical Issues of Wireless-Based Obstacle Mapping

So far we established that the total number of available channel measurements should be distributed over a small number of angles, bigger than or equal to the number of jump angles, with a preference given to the angles of jumps. This, however, assumes that there are no environmental, computational or hardware constraints in implementing both approaches. In case of environmental constraints, the random case has a clear advantage. In such cases, partial coordinated measurements can be taken, within the limits of environmental constraints, in addition to random measurements. Both the random and coordinated cases require communication of position information for antenna alignment. Furthermore, they need narrow beamwidth antennas, to limit multipath fading (see Fig. 3). The random case, however, also requires a constant control and adaptation of the antenna angles to maintain the alignment. Thus, it needs a more advanced hardware. The coordinated case, on the other hand, requires coordinated movement of the robots. Finally, the computational complexity of solving for the map is lower, using the coordinated approach. In summary, we envision that both approaches will be used in practice, depending on the operation environment and the available hardware/software resources.

V. Conclusions

In this paper, we considered wireless-based cooperative mapping of obstacles in a robotic network. Our goal was to thoroughly understand and compare the performance of the random and coordinated wireless sampling approaches, using both simulation and experimental results. We showed that the right way for comparing the performance of these two wireless sampling patterns is to consider the relationship between the reconstruction quality and the angular directions where the map is sampled. More specifically, we established that the total number of available channel measurements should be distributed over a small number of angles (bigger than or equal to the number of jump angles of the structure), with a preference given to the angles of jumps. Finally, we validated our findings by mapping an occluded structure on our campus using our robotic testbed.

VI. Acknowledgments

The authors would like to thank Mehrzad Malmirchegini for helpful discussions.

References

[1] Y. Mostofi and A. Gonzalez-Ruiz. Compressive cooperative obstacle mapping in mobile networks. In *Proceedings of the 29th Military Communications Conference (Milcom)*, pages 947–953, San Jose, CA, nov. 2010.

[2] I. F. Akyildiz, S. Weilian, Y. Sankarasubramaniam, and E. Cayirci. A Survey on Sensor Networks. *IEEE Communications Magazine*, 40(8):102 – 114, August 2002.

[3] V. Kumar, D. Rus, and S. Singh. Robot and Sensor Networks for First Responders . *IEEE Pervasive Computing*, pages 24–33, October-December 2004.

[4] W. B. Heinzelman, A. P. Chandrakasan, and H. Balakrishnan. An Application-Specific Protocol Architecture for Wireless Microsensor Networks. *IEEE Transactions on Wireless Communications*, 1(4):660 – 670, October 2002.

[5] Hao Jiang, Lijia Chen, Jing Wu, Siyue Chen, and H. Leung. A reliable and high-bandwidth multihop wireless sensor network for mine tunnel monitoring. *IEEE Sensors Journal*, 9(11):1511 –1517, nov. 2009.

[6] Nojeong Heo and P.K. Varshney. Energy-efficient deployment of intelligent mobile sensor networks. *IEEE Transactions on Systems, Man and Cybernetics, Part A: Systems and Humans*, 35(1):78 – 92, jan. 2005.

[7] C. Chong and S. Kumar. Sensor networks: evolution, opportunities and challenges. *Proceedings of the IEEE*, 91(8):1247–1256, August 2003.

[8] Boon-Chong Seet, Qing Zhang, Chuan Heng Foh, and A.C.M. Fong. Hybrid RF mapping and kalman filtered spring relaxation for sensor network localization. *IEEE Sensors Journal*, 12(5):1427 –1435, may 2012.

[9] T. Melodia, D. Pompili, V.C. Gungor, and I.F. Akyildiz. Communication and coordination in wireless sensor and actor networks. *IEEE Transactions on Mobile Computing*, 6(10):1116 –1129, oct. 2007.

[10] M. Anisetti, C.A. Ardagna, V. Bellandi, E. Damiani, and S. Reale. Map-based location and tracking in multipath outdoor mobile networks. *IEEE Transactions on Wireless Communications*, 10(3):814 –824, march 2011.

[11] K. Baumgartner, S. Ferrari, and T.A. Wettergren. Robust deployment of dynamic sensor networks for cooperative track detection. *IEEE Sensors Journal*, 9(9):1029 –1048, sept. 2009.

[12] Chia-Ho Ou. A localization scheme for wireless sensor networks using mobile anchors with directional antennas. *IEEE Sensors Journal*, 11(7):1607 –1616, july 2011.

[13] Jingjing Gu, Songcan Chen, and Tingkai Sun. Localization with incompletely paired data in complex wireless sensor network. *IEEE Transactions on Wireless Communications*, 10(9):2841 –2849, september 2011.

[14] Md.A. Rahman, Md.S. Miah, W. Gueaieb, and A.E. Saddik. SENORA: A P2P service-oriented framework for collaborative multirobot sensor networks. *IEEE Sensors Journal*, 7(5):658 –666, may 2007.

[15] H. Durrant-Whyte and T. Bailey. Simultaneous localization and mapping: part I. *IEEE Robotics Automation Magazine*, 13(2):99 –110, june 2006.

[16] T.A. Vidal-Calleja, A. Sanfeliu, and J. Andrade-Cetto. Action selection for single-camera SLAM. *IEEE Transactions on Systems, Man, and Cybernetics, Part B: Cybernetics*, 40(6):1567 –1581, dec. 2010.

[17] F. Dellaert, F. Alegre, and E. B. Martinson. Intrinsic localization and mapping with 2 applications: Diffusion mapping and macro polo localization. In *IEEE Intl. Conf. on Robotics and Automation*, volume 2, pages 2344 – 2349, 2003.

[18] R. Sim, G. Dudek, and N. Roy. A closed form solution to the single degree of freedom simultaneous localisation and map building (SLAM) problem. In *IEEE Conference on Decision and Control*, volume 1, pages 191–196, 2000.

[19] Sebastian Thrun, Wolfram Burgard, and Dieter Fox. *Probabilistic Robotics*. MIT Press, 2001.

[20] R. Gartshore, A. Aguado, and C. Galambos. Incremental map building using an occupancy grid for an autonomous monocular robot. In *7th Intl. Conf. on Control, Automation, Robotics and Vision*, volume 2, pages 613–618, Dec. 2002.

[21] G. Oriolo, G. Ulivi, and M. Vendittelli. Real-time map building and navigation for autonomous robots in unknown environments. *IEEE Transactions on Systems, Man, and Cybernetics, Part B: Cybernetics*, 28(3):316 –333, jun 1998.

[22] W. C. Jakes. *Microwave Mobile Communications*. Wiley-IEEE Press, New York, 1994.

[23] Y. Mostofi and P. Sen. Compressive Cooperative Mapping in Mobile Networks. In *Proceedings of the 28th American Control Conference (ACC)*, pages 3397–3404, St. Louis, MO, June 2009.

[24] Y. Mostofi. Compressive cooperative obstacle/object mapping and see-through capabilities in robotic networks. accepted to appear, IEEE Transactions on Mobile Computing, 2012.

[25] Y. Mostofi. Compressive cooperative sensing and mapping in mobile networks. *IEEE Transactions on Mobile Computing*, 10(12):1769 –1784, dec. 2011.

[26] M. C. Wicks. RF tomography with application to ground penetrating radar. In *Asilomar Conference on Signals, Systems and Computers*, pages 2017–2022, November 2007.

[27] J. Wilson and N. Patwari. Radio tomographic imaging with wireless networks. *IEEE Transactions on Mobile Computing*, 9(5):621 –632, may 2010.

[28] M. Kanso and M. Rabbat. Compressed RF tomography for wireless sensor networks: Centralized and decentralized approaches. In *IEEE Intl. Conference on Distributed Computing in Sensor Systems*, June 2009.

[29] E. Candès, J. Romberg, and T. Tao. Robust uncertainty principles: exact signal reconstruction from highly incomplete frequency information. *IEEE Trans. on Information Theory*, 52(2):489–509, February 2006.

[30] D. L. Donoho. Compressed sensing. *IEEE Transactions on Information Theory*, 52(4):1289–1306, April 2006.

[31] D. Needell and R. Vershynin. Signal recovery from incomplete and inaccurate measurements via regularized orthogonal matching pursuit. *Selected Topics in Signal Processing, IEEE Journal of*, 4(2):310 –316, april 2010.

[32] ℓ_1 magic toolbox. http://www.acm.caltech.edu/l1magic/.

[33] Chengbo Li. *An Efficient Algorithm For Total Variation Regularization with Applications to the Single Pixel Camera and Compressive Sensing*. PhD thesis, RICE University, 2009.

[34] Y. Wang, J. Yang, W. Yin, and Y. Zhang. A new alternating minimization algorithm for total variation image reconstruction. *SIAM J. on Imaging Sciences*, 1(3):248272, 2008.

[35] L. I. Rudin, S. Osher, and E. Fatemi. Nonlinear total variation based noise removal algorithms. *Physica D*, 60:259–268, November 1992.

[36] J. Romberg. Compressive sensing by random convolution. *SIAM Journal on Imaging Science*, December 2009.

[37] D. Strong and T. Chan. Edge-preserving and scale-dependent properties of total variation regularization. *Inverse Problems*, 19(6):S165, 2003.

[38] A. Goldsmith. *Wireless Communications*. Cambridge University Press, 2005.

[39] Y. Mostofi, A. Gonzalez-Ruiz, A. Ghaffarkhah, and D. Li. Characterization and Modeling of Wireless Channels for Networked Robotic and Control Systems - A Comprehensive Overview. In *Proceedings of 2009 IEEE/RSJ International Conference on Intelligent Robots and Systems (IROS)*, St. Louis, MO, October 2009.

[40] A. Gonzalez-Ruiz, A. Ghaffarkhah, and Y. Mostofi. A Comprehensive Overview and Characterization of Wireless Channels for Networked Robotic and Control Systems. *Journal of Robotics*, 2011, 2011.

[41] MobileRobots Inc., 2009. http://www.mobilerobots.com.

[42] Laird Technologies, 2010. http://www.lairdtech.com/Products/Antennas-and-Reception-Solutions/.

Alejandro Gonzalez-Ruiz received the B.S. degree in electronics engineering of the Universidad del Valle de Guatemala, Guatemala City, Guatemala, in 2006, and the M.S. degree in electrical engineering from the University of New Mexico, Albuquerque, NM in 2009. He is currently a visiting researcher at the Department of Electrical and Computer Engineering at the University of California Santa Barbara where he is completing his work towards a Ph.D. from the University of New Mexico.

From 2006 to 2007 he worked for TECO Energy in Guatemala. He received a scholarship from TECO Energy for his undergraduate studies in 2001. In 2007 he was awarded a Fulbright scholarship. His current research interests include compressive and cooperative sensing and control, through-the-wall mapping, and wireless communications. He is a member of the IEEE.

Yasamin Mostofi received the B.S. degree in electrical engineering from Sharif University of Technology, Tehran, Iran, in 1997, and the M.S. and Ph.D. degrees in the area of wireless communication systems from Stanford University, Stanford, CA, in 1999 and 2004, respectively. She is currently an associate professor in the Department of Electrical and Computer Engineering at the University of California Santa Barbara. Dr. Mostofi is the recipient of the 2011 Presidential Early Career Award for Scientists and Engineers (PECASE), the National Science Foundation (NSF) CAREER award, the 2012 IEEE Region 6 Outstanding Engineer Award, and the Bellcore fellow-advisor award from Stanford Center for Telecommunications in 1999, among other awards. She has served on the Control Systems Society conference editorial board since 2008. Her current research lies at the intersection of the two areas of communications and control in mobile sensor networks. Current research thrusts include communication-aware navigation and decision making in robotic networks, compressive sensing and control, obstacle mapping, robotic routers, and cooperative information processing.